Cell Metabolism
Article

Skeletal Muscle-Specific Ablation of *raptor*, but Not of *rictor*, Causes Metabolic Changes and Results in Muscle Dystrophy

C. Florian Bentzinger,[1] Klaas Romanino,[1] Dimitri Cloëtta,[1] Shuo Lin,[1] Joseph B. Mascarenhas,[1] Filippo Oliveri,[1] Jinyu Xia,[2] Emilio Casanova,[3] Céline F. Costa,[1] Marijke Brink,[3] Francesco Zorzato,[2] Michael N. Hall,[1] and Markus A. Rüegg[1,*]
[1]Biozentrum, University of Basel, CH-4056 Basel, Switzerland
[2]Departments of Anesthesia and Biomedicine, Basel University Hospital, CH-4031 Basel, Switzerland
[3]Institute of Physiology, Department of Biomedicine, University of Basel, CH-4056, Basel, Switzerland
*Correspondence: markus-a.ruegg@unibas.ch
DOI 10.1016/j.cmet.2008.10.002

SUMMARY

Mammalian target of rapamycin (mTOR) is a central controller of cell growth. mTOR assembles into two distinct multiprotein complexes called mTOR complex 1 (mTORC1) and mTORC2. Here we show that the mTORC1 component raptor is critical for muscle function and prolonged survival. In contrast, muscles lacking the mTORC2 component rictor are indistinguishable from wild-type controls. Raptor-deficient muscles become progressively dystrophic, are impaired in their oxidative capacity, and contain increased glycogen stores, but they express structural components indicative of oxidative muscle fibers. Biochemical analysis indicates that these changes are probably due to loss of activation of direct downstream targets of mTORC1, downregulation of genes involved in mitochondrial biogenesis, including PGC1α, and hyperactivation of PKB/Akt. Finally, we show that activation of PKB/Akt does not require mTORC2. Together, these results demonstrate that muscle mTORC1 has an unexpected role in the regulation of the metabolic properties and that its function is essential for life.

INTRODUCTION

Growth of an organ during development and during adaptation in the adult can be controlled by alterations in either the number or the size of cells. The two mechanisms are fundamentally different and require distinct regulation. Rapamycin is a cell growth inhibitor used to treat a number of clinical indications including graft rejection and cancer (Tsang et al., 2007). The molecular target of rapamycin is a Ser/Thr kinase, called TOR in yeast (Heitman et al., 1991) or mTOR in mammals. The evolutionarily conserved TOR pathway controls many cellular processes, including protein synthesis, ribosome biogenesis, nutrient transport, and autophagy (reviewed in Wullschleger et al., 2006). mTOR assembles into two distinct multiprotein complexes, termed mTORC1 and mTORC2 (Jacinto et al., 2004; Sarbassov et al., 2004). mTORC1 consists of raptor (*r*egulatory *a*ssociated *p*rotein of m*TOR*), mLST8, PRAS40, and mTOR (Wullschleger et al., 2006) and is sensitive to rapamycin. mTORC2 consists of rictor (*r*apamycin *i*nsensitive *c*ompanion of m*TOR*), mSIN1, mLST8, and mTOR (Jacinto et al., 2004; Sarbassov et al., 2004).

Changes in the size of adult muscle, in response to external stimuli, are mainly due to the growth of individual muscle fibers and not an increase in fiber number (Glass, 2005). As mTOR controls cell growth, it has also been implicated in the control of muscle mass. For example, rapamycin inhibits recovery of skeletal muscle from atrophy (Bodine et al., 2001). Moreover, activation of the mTORC1-upstream component PKB/Akt induces muscle hypertrophy (Bodine et al., 2001; Pallafacchina et al., 2002; Izumiya et al., 2008), and this increase is rapamycin sensitive (Izumiya et al., 2008). Conversely, muscle fibers of mice deficient for the mTOR downstream target S6 kinase 1 (S6K1) are atrophic (Ohanna et al., 2005). In contrast, little is known of the function of rapamycin-insensitive mTORC2, whose primary readouts are thought to be the organization of the actin cytoskeleton. Moreover, mTORC2 has been shown to be the kinase that phosphorylates PKB/Akt on Ser473 (Sarbassov et al., 2005).

To circumvent the early embryonic lethality of mice deficient for raptor or rictor (Guertin et al., 2006; Shiota et al., 2006), we generated mice with floxed *raptor* or *rictor* alleles. Here we describe the phenotype of mice that lack raptor (i.e., mTORC1), rictor (i.e., mTORC2), or both proteins specifically in skeletal muscle. We find that deletion of mTORC2 does not cause an overt muscle phenotype. In contrast, mTORC1-deficient muscles manifest signs of atrophy and become progressively dystrophic. Moreover, muscles behave metabolically like fast-twitch, glycolytic skeletal muscle but exhibit structural features and contraction properties indicative of slow-twitch, oxidative muscle fibers. Biochemical analysis indicates that this phenotype can be accounted for by the absence of phosphorylation of the immediate mTORC1 downstream targets S6K/S6 and 4EBP1, the downregulation of PGC1α, and hyperphosphorylation of PKB/Akt. Finally, deficiency of both raptor and rictor results in a phenotype indistinguishable from that of muscles lacking only raptor. Importantly, PKB/Akt is still hyperphosphorylated under these conditions, suggesting that mTORC2 is not the only kinase able to phosphorylate PKB/Akt on Ser473.

RESULTS

Skeletal Muscle-Specific Ablation of *raptor* and *rictor*

To examine the function of raptor and rictor in skeletal muscle we used the Cre-loxP recombination system. To this end, we introduced loxP sites into the *raptor* locus and the *rictor* locus (Figure 1A). In

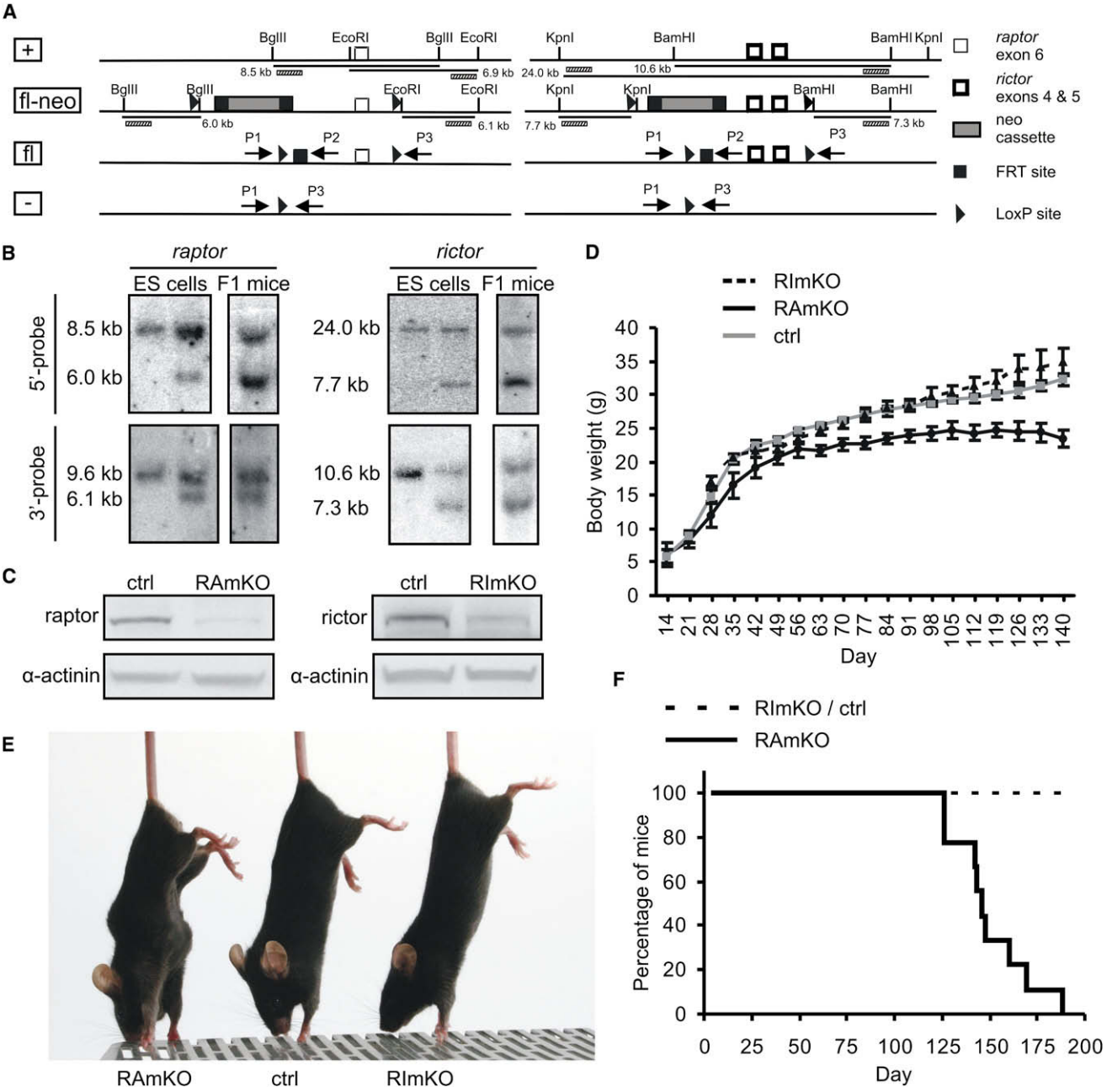

Figure 1. Targeting Strategy and Initial Characterization of RAmKO and RImKO Mice

(A) Schematic presentation of wild-type and targeted alleles of *raptor* (left panel) and *rictor* (right panel) before and after recombination. Localization and size of DNA fragments generated by particular restriction digests are indicated. Probes used for Southern blot analysis are shown by hatched bars. PCR primers for genotyping are indicated by arrows. +: wild-type allele; fl-neo: targeted allele; fl: alleles after recombination by Flp; -: alleles after recombination by Cre.

(B) Southern blot analysis of genomic DNA from ES cells and F1 progeny of resulting chimeras. Correct targeting of the 5′ end is indicated by the presence of a 6.0 kb band in the *raptor* locus and a 7.3 kb band in the *rictor* locus. Correct targeting at the 3′ end is indicated by a 6.1 kb band and a 7.3 kb band. In each blot of ES cells, wild-type is to the left.

(C) Western blot analysis of protein extracts from skeletal muscle of RAmKO and RImKO mice. Controls correspond to muscle extracts from mice that carry the floxed alleles but are negative for *HSA-Cre*. Equal protein loading is confirmed by blotting for α-actinin.

(D) Growth curve of RAmKO, RImKO, and control mice. Mice of each genotype were weighed every week. A significant difference between RAmKO and control mice ($p < 0.05$) was observed after the age of 63 days. Individual data points represent means ± SEM (n = 5 for RAmKO; n = 3 for RImKO; n = 10 for controls).

(E) Photograph of 140-day-old RAmKO, control (ctrl), and RImKO mice.

(F) Survival curve of RAmKO, RImKO, and control mice.

Table 1. Analysis of Particular Tissues in Control and RAmKO Mice

	90 day		140 day	
	ctrl	RAmKO	ctrl	RAmKO
Tibia length (cm)	2.0 ± 0.1	2.0 ± 0.1	2.0 ± 0.1	2.1 ± 0.1
Lower hindleg (mg)	449.2 ± 19.3	344.0 ± 11.4***	428.0 ± 28.0	331.6 ± 41.3**
Triceps brachii (mg)	98.3 ± 11.3	67.0 ± 10.4***	89.5 ± 14.0	68.8 ± 13.8*
Soleus (mg)	9.7 ± 0.8	7.4 ± 0.6***	9.2 ± 0.8	7.1 ± 1.2*
EDL (mg)	12.7 ± 0.8	10.3 ± 0.7***	12.0 ± 0.7	9.4 ± 1.4*
Tibialis anterior (mg)	58.3 ± 2.7	40.8 ± 2.3***	55.6 ± 1.8	39.0 ± 1.3***
Epididymal fat pad (mg)	566.4 ± 214.9	438.9 ± 93.1	616.0 ± 194.8	242.5 ± 118.7**
Heart (mg)	85.12 ± 6.6	68.1 ± 4.1*	88.5 ± 2.1	72.1 ± 4.4**
Liver (mg)	1350.9 ± 185.0	1187.5 ± 161.0	1232.0 ± 187.5	1055.0 ± 269.1

Weight or length was measured for different muscles, bones, and other organs in 90- and 140-day-old mice. p values determined by Student's t test are indicated by asterisks (n = 4 mice). Values represent means ± SD. *$p < 0.05$, **$p < 0.01$, ***$p < 0.001$.

both cases, Cre-mediated recombination causes a frame shift and early stop of translation. In addition, Flp recognition target (FRT) sites were inserted that flanked a neomycin resistance cassette for the selection of targeted embryonic stem (ES) cells. This cassette was removed using Flp deleter mice (Figure 1A; Rodriguez et al., 2000). Southern blot analysis confirmed successful targeting in ES cells and germline transmission of resulting chimeras (Figure 1B). Mice homozygous for the floxed allele (*raptor*$^{fl/fl}$ or *rictor*$^{fl/fl}$) were mated with heterozygous floxed mice that also expressed Cre recombinase under the control of the muscle-specific human skeletal actin (HSA) promoter (Schwander et al., 2003). Mice positive for the *HSA-Cre* transgene that also carried two floxed alleles were then analyzed. For simplicity, we refer to *HSA-Cre*; *raptor*$^{fl/fl}$ as RAmKO (for *ra*ptor *m*uscle *k*nock*o*ut) and to *HSA-Cre*; *rictor*$^{fl/fl}$ as RImKO (for *ric*tor *m*uscle *k*nock*o*ut) mice. Successful recombination of *raptor* or *rictor* was confirmed by PCR on genomic DNA isolated from tibialis muscle (Figure S1A available online). Western blot analysis of RAmKO and RImKO skeletal muscle revealed a strong reduction of the respective proteins (Figures 1C and S1B; Table S1). Residual expression of these proteins in knockout muscle is not due to leaky recombination of the targeted allele as *raptor*$^{fl/fl}$ or *rictor*$^{fl/fl}$ mice crossed to other Cre-expressing mice led to a complete loss of the respective protein in the targeted tissue (Figure S1B; Polak et al., 2008; M.N. Hall, personal communication). Thus, the low levels of raptor and rictor protein that were detected in the RAmKO and RImKO muscles are ascribable to the expression of raptor or rictor in nontargeted cells, such as fibroblasts, satellite cells, Schwann cells, and peripheral nerves, which are also contained in skeletal muscle.

Neither RAmKO nor RImKO mice showed an overt phenotype in the first weeks of life. Starting at the age of approximately 5 weeks, RAmKO mice could be distinguished from their littermates by their lower body weight. The difference became significant after day 63, and the mice remained lighter throughout life (Figure 1D). In contrast, the body weight of RImKO mice did not differ significantly from controls, although at higher age RImKO mice were slightly heavier (Figure 1D). For both RAmKO and RImKO mice, the food consumption was comparable to controls (Figure S1C and data not shown). RAmKO mice developed a pronounced kyphosis starting at the age of approximately 2 months and became markedly lean (Figures 1E and S1D). In contrast, RImKO mice appeared normal. Finally, RAmKO mice began to die at the age of 110 days, and none survived for more than 190 days (Figure 1F). RImKO mice did not die prematurely (the oldest RImKO mice now being more than 2 years old).

To examine whether the difference in weight gain was based on reduced muscle mass in RAmKO mice, we weighed different muscles and several other organs at day 90 (i.e., before the mice showed a severe phenotype) and at day 140. As shown in Table 1, all the muscles measured were significantly lighter in 90- and 140-day-old RAmKO mice compared to controls. As RAmKO mice appeared lean (Figure 1E) and only little or no fat was detected in older mice (Figure S1D), we also weighed the epididymal fat pads. Indeed, RAmKO mice contained significantly less adipose tissue at the age of 140 days (Table 1). The loss of adipose tissue does not seem to be due to changes in mitochondrial uncoupling properties as the body temperature of RAmKO mice was not different from those of control littermates (Figure S1E). The weight of the liver was indistinguishable from controls whereas hearts were again lighter (Table 1). The left ventricle mass of the heart, however, correlated with the difference in body weight (Figure S1F), indicating that the difference in heart weight is probably due to allometric scaling (Popovic et al., 2005). Moreover, the ejection fraction determined by echocardiography was indistinguishable from littermate controls (data not shown). Finally, we could not detect any recombination events in the hearts of RAmKO mice (Figure S1A). Our data therefore show that raptor deficiency in skeletal muscle causes a progressive, disproportional loss of skeletal muscle and fat.

Deficiency of mTORC1 but Not mTORC2 Causes Muscle Dystrophy

Kyphosis and early death are often signs of muscle dystrophy (Laws and Hoey, 2004). We therefore examined different skeletal muscles of RAmKO and RImKO mice using hematoxylin and eosin (H&E) staining. No change in the overall architecture of soleus and extensor digitorum longus (EDL) muscles was found in RImKO mice (Figure 2A). Muscles from RAmKO mice showed

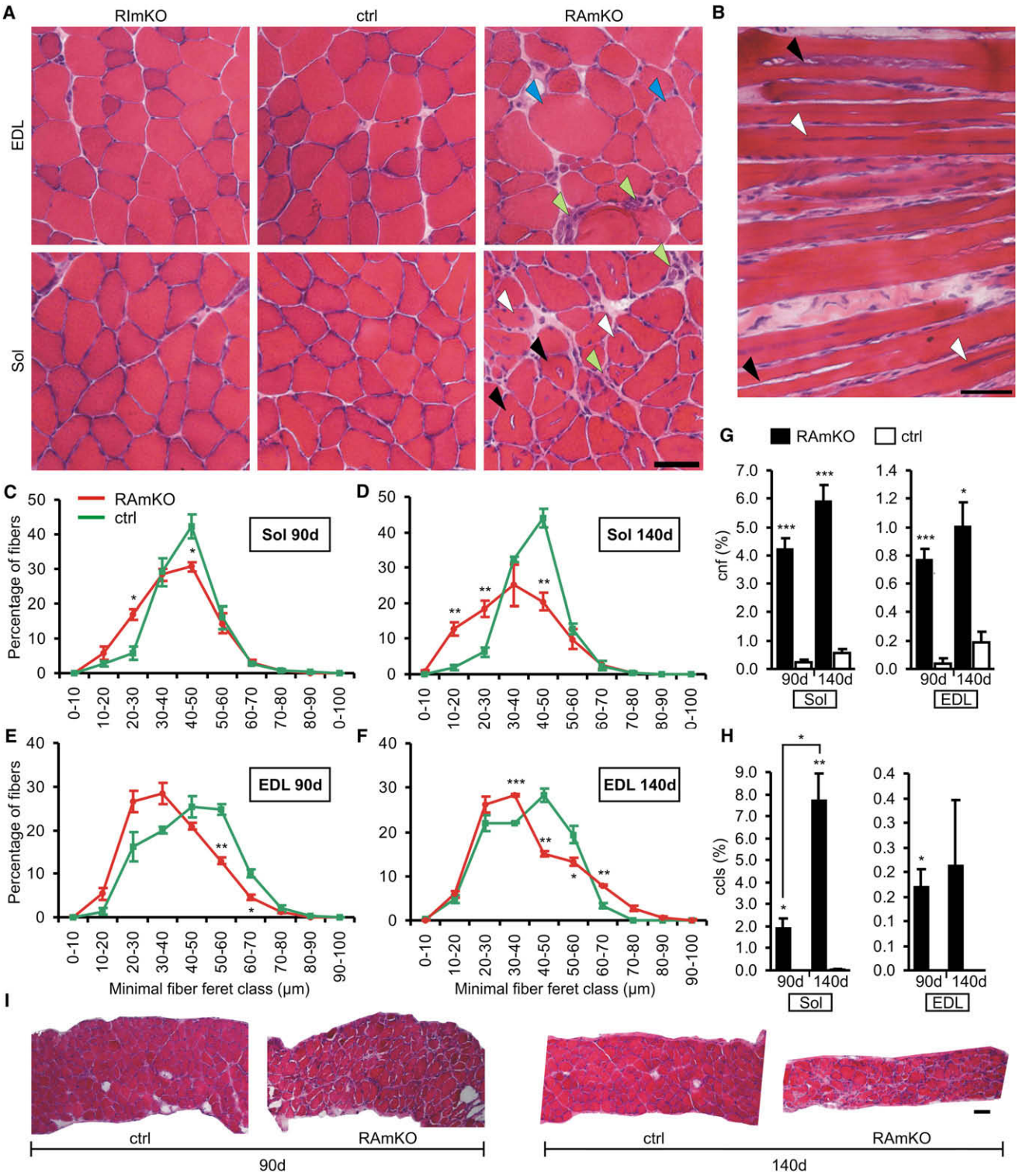

Figure 2. Muscles of RAmKO Mice Show Signs of a Progressive Dystrophy

(A) Hematoxylin and eosin (H&E) staining of muscle cross-sections from the EDL and soleus (Sol) muscle of 140-day-old mice. In EDL muscle of RAmKO mice, some large (blue arrowheads) but also small fibers are present. Centralized nuclei (white arrowheads) and central core-like structures (black arrowheads) can be found in soleus muscle of RAmKO mice. Both muscles contain many mononuclear cells (green arrowheads).

(B) Longitudinal section of soleus muscle of a 140-day-old RAmKO mouse. Besides centrally aligned nuclei (white arrowheads), central core-like structures (black arrowheads), which expand longitudinally in muscle fibers, are visible.

(C–F) Fiber size distribution in the soleus muscle of 90-day- (C) and 140-day-old (D) and in the EDL muscle of 90-day- (E) and 140-day-old (F) RAmKO and control mice.

signs of a dystrophy, such as mononuclear cells (green arrowheads) and a high number of small and large muscle fibers (blue arrowheads). In soleus muscle and to a lower extent in EDL, we also found muscle fibers with centralized nuclei (white arrowheads), indicative of ongoing de- and regeneration, and structures reminiscent of central cores (black arrowheads in Figures 2A and 2B). Quantification showed that the fiber size distribution was strongly altered in both soleus and EDL muscle (Figures 2C–2F). In addition, the number of centralized myonuclei (Figure 2G) and the relative percentage of muscle fibers with the central core-like structures (Figure 2H) were higher in RAmKO mice compared to controls. Dystrophic hallmarks seemed more pronounced in soleus than in EDL muscle. Interestingly, the severity of the dystrophy correlated with the high endogenous expression of raptor, rictor, mTOR, or PKB/Akt in wild-type soleus muscle (Figure S2A). Muscles of RAmKO mice also showed increased immunoreactivity for tenascin-c and f4/80 (Figure S2B), which mark fibrotic tissue (Ringelmann et al., 1999) and infiltrating macrophages (Austyn and Gordon, 1981), respectively. However, other dystrophic hallmarks including increased uptake of Evans blue into muscle fibers and increased levels of creatine kinase in the blood could not be detected (Figure S2C and data not shown). Similarly, the number of muscle fibers was not changed in soleus muscle of RAmKO mice compared to controls (Figure S2D). Neuromuscular junctions of RAmKO mice were indistinguishable from those in control mice (Figure S2E). Probably due to ongoing de- and regeneration, many extrasynaptic acetylcholine receptor (AChR) clusters could be detected in the diaphragm of RAmKO mice (Figure S2F). Based on the extensive muscle wasting and the high degree of fibrosis, the dystrophy was particularly severe in the diaphragm of older mice (Figure 2I), suggesting that respiratory failure might be the cause of premature death. In contrast to RAmKO mice, muscles of RImKO mice did not show any alterations in fiber size (Figure S3A) and in the cytoskeletal organization as indicated by the sarcomeric arrangement of α-actinin (Figure S3B). In summary, our data show that ablation of *raptor* and thus of mTORC1, but not of *rictor*, results in a progressive muscle dystrophy.

Skeletal Muscles of RAmKO Mice Show Alterations in Their Metabolic and Structural Properties

One of the first observations we made during the course of this work was that muscles of RAmKO mice appeared paler than those of RImKO or control mice. This difference was particularly striking for the soleus muscle (Figure 3A, arrowhead) and was not based on decreased vascularization, as revealed by staining for laminin-α5 (data not shown), which is expressed in blood vessels (Sorokin et al., 1997). To test for changes in mitochondrial function, we used an NADH-tetrazolium (NADH-TR) staining. Indeed, the activity of oxidative enzymes appeared lower in both EDL and soleus muscles of RAmKO mice (Figure 3B). Fibers with central core-like structures, which were completely devoid of NADH-TR reactivity, could be found in RAmKO soleus muscle (black arrowheads). Such a lack of NADH staining is a diagnostic feature of central core disease (Sewry et al., 2002). To further test whether the changes in NADH-TR reactivity involved mitochondria, we also examined longitudinal sections of soleus muscle by electron microscopy. Muscle of RAmKO mice was distinguishable from control muscle by a substantial loss of intermyofibrillar mitochondria, which are normally localized perpendicular to the Z disks (arrows in upper panel, Figure 3C). Only few intermyofibrillar mitochondria remained (arrow lower panel, Figure 3C). Moreover, mitochondria localized in the subsarcolemmal space seemed more densely packed and swollen in RAmKO mice (Figure S4A). As a decrease in oxidative properties is often accompanied by a compensatory increase in glycolytic activity, we performed a periodic acid-Schiff (PAS) staining. Indeed, the glycogen content was increased in both EDL and soleus muscle (Figure 3D). The increase was more pronounced in the fast-twitch EDL muscle. The glycogen content in the *gastrocnemius* muscle, which consists of a mixed population of fast- and slow-twitch fibers, was more than five times higher than in control mice (control: 21 ± 7 μmol glucose/g tissue; RAmKO: 108 ± 22 μmol glucose/g tissue; mean ± SEM; n = 4 mice). The change in oxidative capacity and glycogen content in skeletal muscle also affected overall metabolism as glucose uptake from the blood was significantly slower in RAmKO mice compared to littermate controls (Figure 3E).

High content of glycogen is indicative of fast-twitch (type II) muscle fibers. To test whether muscles in RAmKO mice also changed their structural properties, we stained EDL and soleus muscle for the slow myosin heavy chain (slMHC), a marker of slow-twitch fibers. Surprisingly, EDL and soleus muscles of 140-day-old RAmKO mice contained even more slMHC-positive muscle fibers (Figure 3F, green) than controls, and the increase of slMHC was regionalized in individual muscles (Figure S4B). In both muscles, the number of slMHC-positive fibers was approximately two to three times higher than in controls (Figures 3G and 3H). In soleus muscle of RAmKO mice, almost 100% of the fibers were positive for slMHC (Figure 3H), and this increase was also seen by western blot analysis (Figure 3I; Table S1). Moreover, other components characteristic for slow-twitch muscle, such as the slow isoform of troponinT (slTnT) and of troponinI (slTnI), were also increased in soleus muscle of RAmKO mice (Figures 3I and 3J; Table S1). Thus, deletion of mTORC1 in skeletal muscle fibers causes a shift of their metabolic properties from oxidative to glycolytic. However, this change in the metabolic characteristics of muscles is opposite to their structural properties.

Functional Characterization of Muscles in RAmKO Mice

To address whether the observed changes in metabolic and structural characteristics had consequences on the overall performance of muscle, we allowed 90-day-old mice to exercise using voluntary wheel running. The representative activity chart of a single mouse shows that running sessions of RAmKO mice were shorter and less frequent than those of controls

(G) Mean percentage of muscle fibers with centralized nuclei (cnf) in the soleus and EDL muscle of RAmKO and control mice.
(H) Percentage of muscle fibers containing central core-like structures (ccls) in soleus and EDL muscle of RAmKO and control mice.
(I) H&E staining of cross-sections of the diaphragms of 90-day- and 140-day-old RAmKO and control mice.
Individual data points and bars (C–H) represent means ± SEM (n = 4 mice). Scale bars (A, B, and I) = 50 μm. p values are ***p < 0.001; **p < 0.01; *p < 0.05.

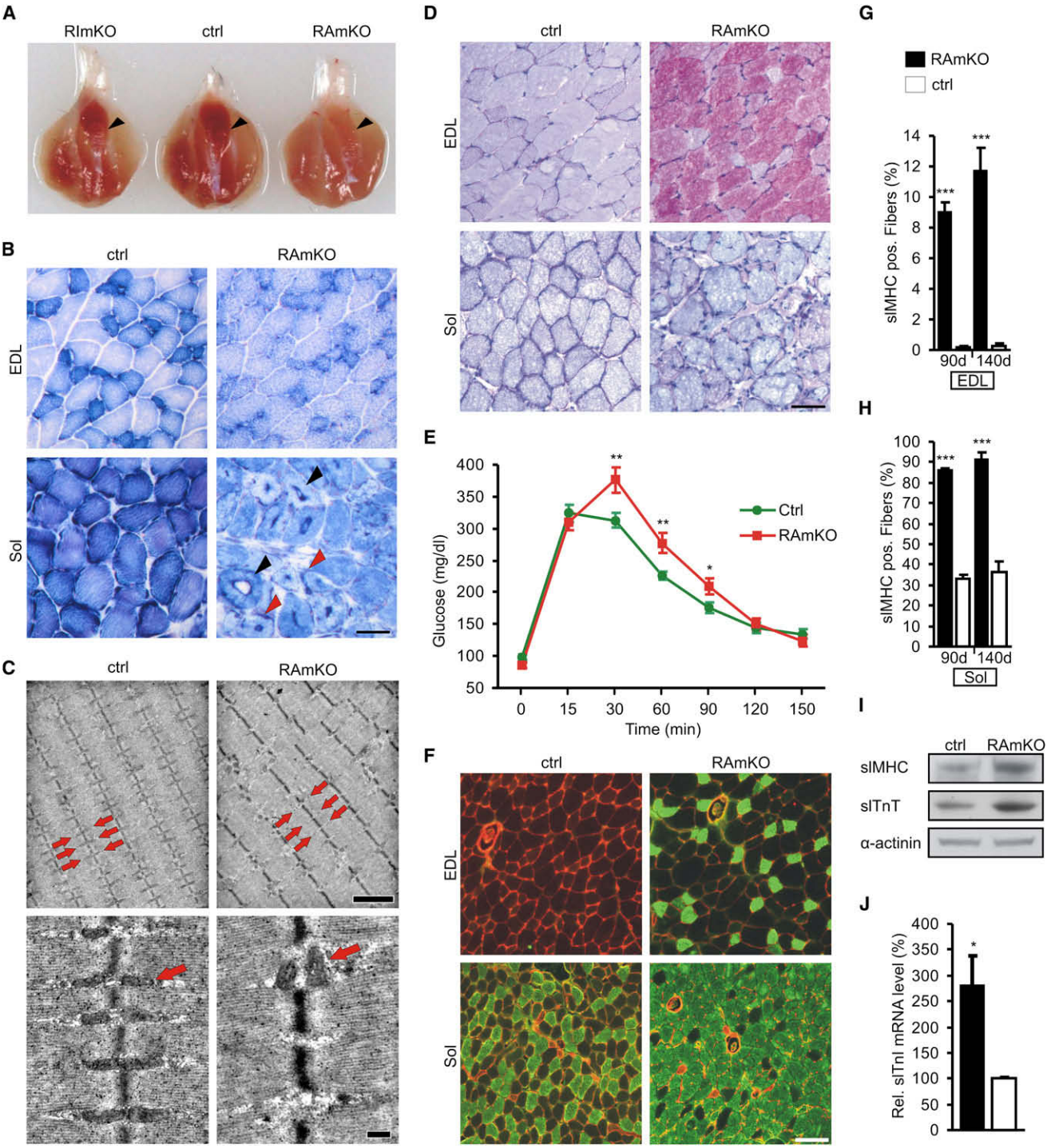

Figure 3. Metabolic and Structural Properties Diverge in Skeletal Muscle of RAmKO Mice

(A) Preparation of the entire hindleg isolated from 90-day-old mice of the genotypes indicated. Note that soleus muscle (arrowheads) is pale in RAmKO mice compared to RImKO and control mice.

(B) Activity of oxidative enzymes examined by NADH-tetrazolium staining (blue precipitate) in EDL and soleus muscle of 140-day-old mice. Central core-like structures devoid of NADH staining (black arrowheads) and increased subsarcolemmal reactivity (red arrowheads) were detected in some RAmKO soleus fibers.

(C) Electron micrographs of longitudinal sections of soleus muscle from 140-day-old mice. Most intermyofibrillar mitochondria in RAmKO muscle are lost from their specific position next to Z disks (red arrows, upper panel). Remaining mitochondria in RAmKO mice show high morphologic variability (red arrow, lower panel).

(D) Periodic acid-Schiff (PAS) staining of cross-sections from 140-day-old mice. The reaction product (magenta color) is indicative of the amount of glycogen in the tissue.

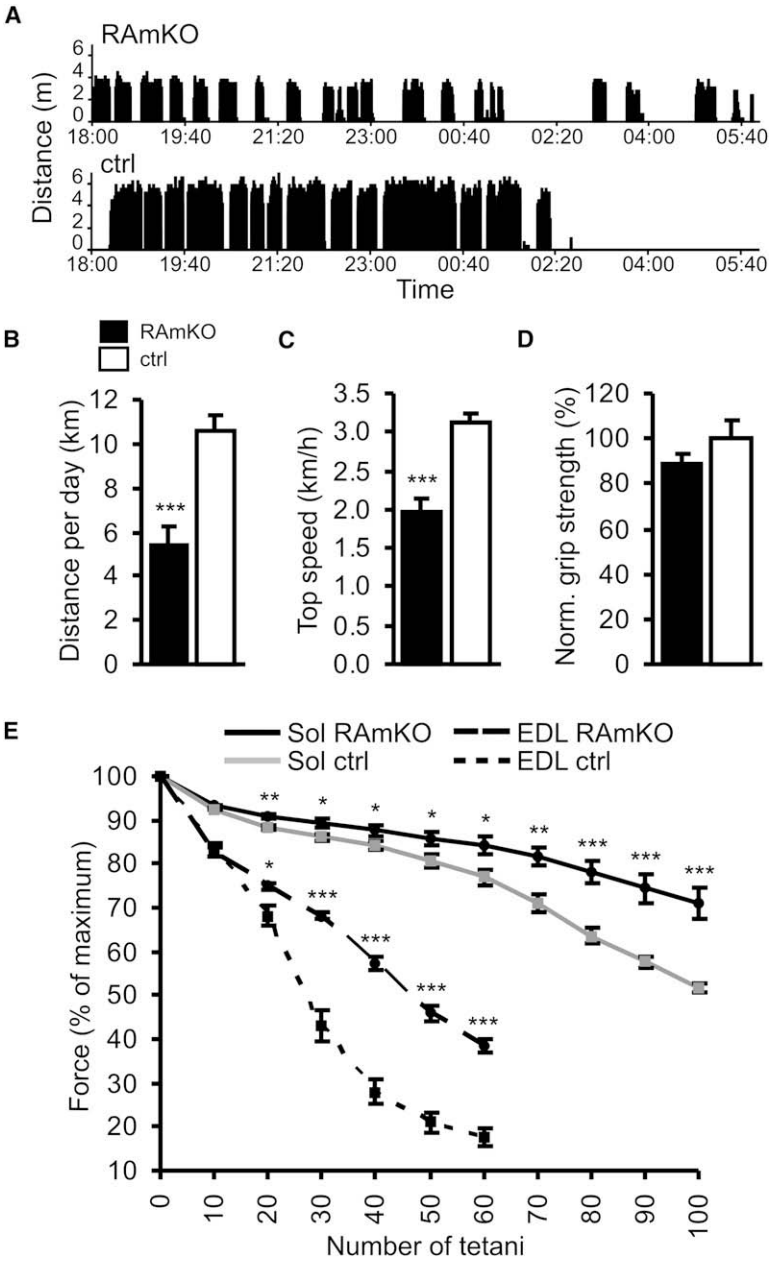

Figure 4. Exercise Performance and Muscle Physiology

(A) Representative activity chart with bins of 10 s from a single 95-day-old RAmKO mouse or a control mouse. Charts were measured from 6 pm to 6 am (dark cycle).

(B) Average distance run per day determined during one week (starting at the age of 90 days, n = 4 for RAmKO and n = 9 for controls).

(C) Average of the top 10% speed measured over one week (starting at the age of 90 days, n = 4 for RAmKO and n = 9 for controls).

(D) Grip strength of 90-day-old RAmKO and control mice. Average time mice were able to hold on a horizontal grid was normalized to body weight. Values of control mice were set to 100% (n = 3).

(E) Force capacity resistance of EDL or soleus muscle isolated from 140-day-old mice was measured during muscle fatigue induced by intermittent tetanic stimulation. Trains of 150 Hz tetani of 350 ms duration were given at 3.6 s intervals (n = 3 for RAmKO and n = 4 for control mice).

Individual data points and bars (B–E) represent means ± SEM. p values are ***p < 0.001; **p < 0.01; *p < 0.05.

(Figure 4A). When averaged over one week, the total distance run per day by RAmKO mice was ~60% of that of control mice (Figure 4B), and the top running speed was significantly lower (Figure 4C). In contrast to the aerobic wheel running task, RAmKO mice performed as well as control animals in a grip strength test on a horizontal grid (Figure 4D). To examine the contraction properties of muscles, force measurements were performed on isolated EDL and soleus muscles. In line with the observed increase of fibers expressing structural proteins characteristic of slow-twitch muscle, time to peak, half time to peak, and relaxation time of the twitch were all increased (Table 2). This difference to control mice did not reach significance in EDL muscle but was highly significant in soleus muscle (Table 2). Twitch force and maximal tetanic absolute force for both muscles were, however, significantly lower in RAmKO mice. The decrease of absolute force capacity reflects the decrease of muscle mass (Table 1) since there is no difference of the maximal tetanic force when normalized to the muscle cross-sectional area (Table 2). An intermittent maximal tetanic stimulation protocol revealed that both EDL and soleus muscles from RAmKO mice were more resistant to fatigue (Figure 4E). These data indicate that raptor-deficient muscle fibers have a reduced aerobic capacity (voluntary wheel running) like fast-twitch, glycolytic muscle fibers but exert contraction properties (isolated muscles) of slow-twitch, oxidative muscle fibers.

Inactivation of *raptor* or *rictor* Affects Activation of PKB/Akt

In search of a mechanistic explanation for the phenotypes, we examined soleus muscle of RAmKO and RImKO mice

(E) Glucose tolerance test with 65-day-old mice (n = 8 for RAmKO and n = 11 for control mice).

(F) Immunostaining for slow myosin heavy chain (slMHC; green) and the laminin γ1 chain (red) of cross-section from 140-day-old mice.

(G and H) Quantification of slMHC-positive muscle fibers in soleus and EDL muscle from 90- and 140-day-old mice (n = 4).

(I) Western blot analysis for slMHC and slow troponin T (slTnT) using soleus muscle of 90-day-old mice. α-actinin is shown as a loading control.

(J) Relative mRNA levels of the slow skeletal muscle troponin I isoform (slTnI) in the soleus of 90-day-old mice as determined by qRT-PCR (n = 3).

Individual data points and bars (E, G, H, and J) represent means ± SEM. Scale bars = 50 μm (B and D), 2 μm (upper pictures, C), 250 nm (lower pictures, C), and 125 μm (F). p values are ***p < 0.001; **p < 0.01; *p < 0.05.

Table 2. Analysis of the Contractile Properties of EDL and Soleus Muscles of Control and RAmKO Mice

	EDL		Sol	
	ctrl	RAmKO	ctrl	RAmKO
Twitch				
Time to peak (ms)	10.1 ± 0.9	11.1 ± 1.2	20.3 ± 4.2	39.7 ± 2.4***
Half time to peak (ms)	3.0 ± 0.4	3.5 ± 0.5	5.6 ± 0.6	11.6 ± 1.1***
Half relaxation time (ms)	15.5 ± 2.2	16.8 ± 3.3	30.8 ± 8.7	63.0 ± 5.1***
Absolute force (mN)	54.0 ± 13.2	45.0 ± 9.7	30.0 ± 5.6	21.0 ± 8.1*
Tetanus				
Half contraction time (ms)	16.6 ± 2.0	14.4 ± 1.1*	27.5 ± 5.4	41.0 ± 5.4***
Half relaxation time (ms)	22.1 ± 1.3	24.1 ± 1.6*	55.2 ± 3.9	124.4 ± 13.2***
Absolute force (mN)	311 ± 57.6	224 ± 38.1**	205 ± 20.8	164.0 ± 42.83
Specific force (mN/mm^2)	380.2 ± 57.2	328.3 ± 62.7	311.6 ± 56.3	264 ± 66.9

Data were recorded from EDL and soleus muscles of 140-day-old mice. p values determined by Student's t test are indicated by asterisks (n = 3 for RAmKO and n = 4 for control mice). Values represent mean ± SD.

biochemically. In each experiment, at least three different mice were compared with three littermate controls. Deletion of *raptor* or *rictor* did not significantly affect the levels of mTOR (Figure 5A; Table S1). The levels of rictor were not lowered in RAmKO mice, and there was a slight decrease of raptor in RImKO mice (Figure 5A; Table S1). The amount of S6K, S6, and 4EBP1, which are the main targets of mTORC1, was not changed in RAmKO mice. However, phosphorylation of S6 and 4EBP1 was strongly decreased (Figure 5A; Table S1). In RImKO mice, mTORC1 targets were not changed, but the level and activation state of PKB/Akt and PKCα, which are both well-characterized substrates of mTORC2 (Sarbassov et al., 2004, 2005), were lower. More importantly, phosphorylation of PKB/Akt on residues Thr308 and Ser473 was strongly increased in RAmKO mice (Figure 5A; Table S1). Furthermore, the total amount of FoxO1 and FoxO3a was increased in RAmKO mice concomitant with an increase in phosphorylation of FoxO1 on Thr24 (Figure 5A; Table S1). In contrast, phosphorylation of FoxO1 on Ser316 and of FoxO3a on Thr32 was not increased.

Activation of S6K by mTORC1 causes feedback inhibition of the insulin/IGF1 pathway by affecting the levels and the phosphorylation of IRS-1 (Um et al., 2004; Harrington et al., 2004). Consistent with this notion, deficiency of mTORC1 and thus absence of S6K/S6 activation abrogated this inhibitory feedback and strongly increased IRS-1 levels in muscles of RAmKO mice (Figure 5B; Table S1). Concomitant with the high protein levels, IRS phosphorylation on Ser636 and Ser639 was increased. On the other hand, there was no significant change in either the levels or the phosphorylation of the mitogen-activated protein kinases Erk1 and Erk2 (Figure 5B; Table S1). Thus, activation of PKB/Akt is probably due to the failure of raptor-deficient muscle fibers to activate S6K and thus due to the absence of the inhibitory feedback onto IRS. The release of this feedback in muscle may require prolonged inactivation of mTORC1 as phosphorylation of PKB/Akt was not increased after 8 hr treatment of cultured C2C12 myotubes with rapamycin and was only slightly elevated after 16 hr (Figure S5C).

Next, we asked whether part of the phenotype of RAmKO mice could be based on this hyperphosphorylation of PKB/Akt. To determine whether PKB/Akt was indeed activated within muscle fibers and not in non-muscle tissue of RAmKO mice, we stained cross-sections of soleus muscle with antibodies specific for PKB/Akt phosphorylated on Ser473 (P-PKB/Akt^{S473}). Indeed, many of the muscle fibers were strongly positive for P-PKB/Akt^{S473} (Figure S5A). Akt/PKB has been shown to regulate expression of atrogenes, called *atrogin-1/MAFbx* and *MuRF-1*, via the FoxOs (Sandri et al., 2004; Stitt et al., 2004). As expected, mRNA levels for both atrogenes were significantly lower in RAmKO mice than in controls (Figure 5C). A further target of PKB/Akt is glycogen synthase kinase3β (GSK3β), which in turn inhibits glycogen synthase (Sakamoto and Goodyear, 2002). Whereas the amount of GSK3β was unaffected, phosphorylation of Ser9 was significantly increased (Figure 5C; Table S1). Moreover, glycogen phosphorylase, which is the enzyme that generates free glucose from glycogen, was downregulated (Figure 5C; Table S1). Thus, hyperphosphorylation of PKB/Akt in conjunction with downregulation of glycogen phosphorylase is probably the basis for the increased levels of glycogen observed in RAmKO mice.

In an attempt to identify the pathway that might underlie the increased number of muscle fibers expressing slMHC, we found a slight increase in the levels of calcineurin and a highly significant increase in myocyte-enhancer factor 2A (Mef2A; Figure 5C; Table S1). A slight, but not significant increase in Mef2D was also observed. The increase in Mef2A is not a consequence of the ongoing de- and regeneration in soleus muscle as Mef2A was also increased in the least affected EDL muscle (Figure S5B). In contrast to skeletal muscle in vivo, Mef2A and slMHC were not increased in cultured C2C12 myotubes upon prolonged treatment with rapamycin (Figure S5C).

Genes Involved in Mitochondrial Biogenesis Are Downregulated in RAmKO Mice

One of the most striking features of RAmKO skeletal muscle is its lower oxidative capacity that is probably due to ultrastructural changes and loss of mitochondria. Thus, we also tested whether genes involved in mitochondrial biogenesis were affected by the deletion of *raptor*. Recent evidence indicates a function of mTORC1 in the regulation of mitochondrial function via PGC1α (Cunningham et al., 2007). Consistent with these findings, transcript levels for PGC1α and for its target gene *myoglobin* were significantly reduced in RAmKO muscle (Figure 5E). Moreover, the protein levels of the PGC1α coactivator PPARγ and the mitochondrial marker cytochrome *c* oxidase IV (COX IV) were significantly decreased in RAmKO mice (Figure 5F; Table S1). These results are consistent with the low oxidative capacity of muscle from RAmKO mice, and they support the notion that this is due to loss of PGC1α.

Activation of PKB/Akt Is Independent of mTORC2

To test whether the hyperactivated state of PKB/Akt in RAmKO mice can be prevented by additional deletion of *rictor*, we generated double floxed mice and mated those with *HSA-Cre* mice. The resulting mice, called DmKO, lacked both raptor and rictor in skeletal muscle (Figure 5G; Table S1). Their overall phenotype was indistinguishable from RAmKO mice (data not shown). Like in RAmKO mice, skeletal muscle of DmKO mice contained high levels of glycogen and was less oxidative (Figure 5H). Levels of mTOR were significantly lower in DmKO mice than in either of the single knockouts (Figure 5G; Table S1). As mTORC2 was shown to phosphorylate PKB/Akt on Ser473 (Sarbassov et al., 2005), we also tested the activation state of PKB/Akt in DmKO muscle. As shown in Figure 5G and in Table S1, PKB/Akt was still hyperphosphorylated on Thr308 and Ser473 in DmKO mice. Again, phosphorylation of PBK/Akt occurred only in muscle fibers and not in non-muscle tissue (Figure 5J). In summary, these results indicate that mTORC2 is not the only kinase that phosphorylates PKB/Akt on Ser473.

DISCUSSION

Our work dissects the role of raptor and rictor (i.e., mTORC1 and mTORC2, respectively) in skeletal muscle. The *HSA-Cre* mice used for our experiments start to express Cre at the earliest stages of skeletal muscle development when the first myotubes are formed. In fully developed muscle, Cre is exclusively expressed in skeletal muscle fibers but not in non-muscle cells, such as Schwann cells, fibroblasts, or satellite cells (Schwander et al., 2003). Neither RAmKO nor RImKO mice showed any abnormalities at birth, indicating that mTORC1 and mTORC2 are not essential for muscle development. Whereas no overt phenotype was detected in RImKO mice throughout adulthood, which is consistent with another report (Kumar et al., 2008), RAmKO mice developed a progressive dystrophy and ultimately died around the age of 5 months. Interestingly, DmKO mice showed very similar pathological changes as RAmKO mice, indicating that mTOR function in skeletal muscle requires only mTORC1.

The dystrophy in RAmKO mice did not affect all muscles to the same extent. For example, diaphragm and soleus muscles were severely affected while EDL showed many fewer changes. Prominent features of the dystrophy were elevated numbers of muscle fibers with centralized nuclei and the presence of central core-like structures. Central cores are hallmarks of "central core diseases," which are inherited neuromuscular disorders with a myopathic syndrome. The most frequent causes of this group of diseases are mutations in the ryanodine receptor, which is the main protein responsible for calcium homeostasis in muscle (reviewed in Treves et al., 2008). Thus, the similarity of the pathology in RAmKO to this class of disease suggests that mishandling of intracellular calcium may underlie the disease. The low levels of PGC1α may additionally contribute to the dystrophic phenotype of RAmKO mice as conditional ablation of *PGC1*α in skeletal muscle results in a myopathic phenotype (Handschin et al., 2007). Finally, several metabolic diseases that cause accumulation of glycogen in skeletal muscle, such as Pompe's and McArdle's diseases, affect skeletal muscle function. The most severely affected patients may even die because of respiratory distress (Winkel et al., 2005). In summary, RAmKO mice show changes in muscle homeostasis that together may lead to the progressive muscle dystrophy.

Raptor Is Required for High Oxidative Capacity of Skeletal Muscle

We found that the severity of the muscle dystrophy correlated with the relative levels of raptor, rictor, mTOR, and PKB/Akt in particular muscles. Interestingly, the most affected muscles, such as soleus or diaphragm, are also those that are insulin sensitive (Song et al., 1999) and contain a high number of slow-twitch, oxidative fibers. Biochemical and morphological analysis showed that soleus muscle expressed little of the oxygen carrier myoglobin and of COX IV and contained fewer and misshaped mitochondria. A direct role of mTOR and raptor for the function of mitochondria has recently been suggested using cultured Jurkat cells (Schieke et al., 2006). Moreover, mTOR has been shown to form a complex with PGC1α (Cunningham et al., 2007), which together with its cofactor PPARγ is a key regulator of mitochondrial biogenesis and function. Consistent with a regulatory function of mTORC1 for mitochondria, mRNA levels for PGC1α and protein levels of PPARγ were decreased in RAmKO mice. Furthermore, mRNA and protein levels of target genes for PGC1α/PPARγ, such as myoglobin (Lin et al., 2002) and glycogen phosphorylase (Wende et al., 2007), were also reduced in RAmKO mice. Also, very similar to the phenotype of RAmKO mice, a reduced intermyofibrillar mitochondrial content in slow-twitch muscles has been reported in PGC1α knockout mice (Leone et al., 2005). In summary, our data indicate that mTORC1 is essential for the function of mitochondria in skeletal muscle, and they link mTORC1 to the regulation of PGC1α in vivo.

Segregation of Metabolic and Structural Properties in Skeletal Muscle of RAmKO Mice

Despite the loss of oxidative capacity and the downregulation of PGC1α, expression of slow structural proteins (slSP; Figure 5K) was increased in RAmKO mice. Analysis of the mechanical properties in EDL and soleus muscle further confirmed that both muscles adapt characteristics indicative of slow-twitch fibers. These results suggest that RAmKO mice induce a structural program for slow-twitch fibers. As muscle-specific inactivation of *PGC1*α causes a fiber-type switch to fast-contracting muscle fibers (Handschin et al., 2007) and transgenic overexpression causes an increase in oxidative muscle (Lin et al., 2002), we also tested whether any other pathways that affect muscle differentiation were altered in the RAmKO mice. Besides PGC1α, the best characterized factors involved in fiber-type determination are calcineurin/NFAT and the Mef2 transcription factors (Bassel-Duby and Olson, 2006). Of those candidate genes, the levels of calcineurin and in particular of Mef2A and Mef2D were increased in RAmKO mice. Thus, facilitated Mef2-mediated transcription may be the basis for the increased levels of slSP despite the low levels of PGC1α. Opposite regulation of PGC1α and Mef2A has also been seen in cultured cells when treated with rapamycin (Cunningham et al., 2007). Mef2 has also been shown to be dominant in the regulation of muscle fiber type as transgenic overexpression of a constitutively active form of Mef2 is sufficient to increase the number of slow muscle fibers (Potthoff et al., 2007). Mef2 is generally thought to be controlled

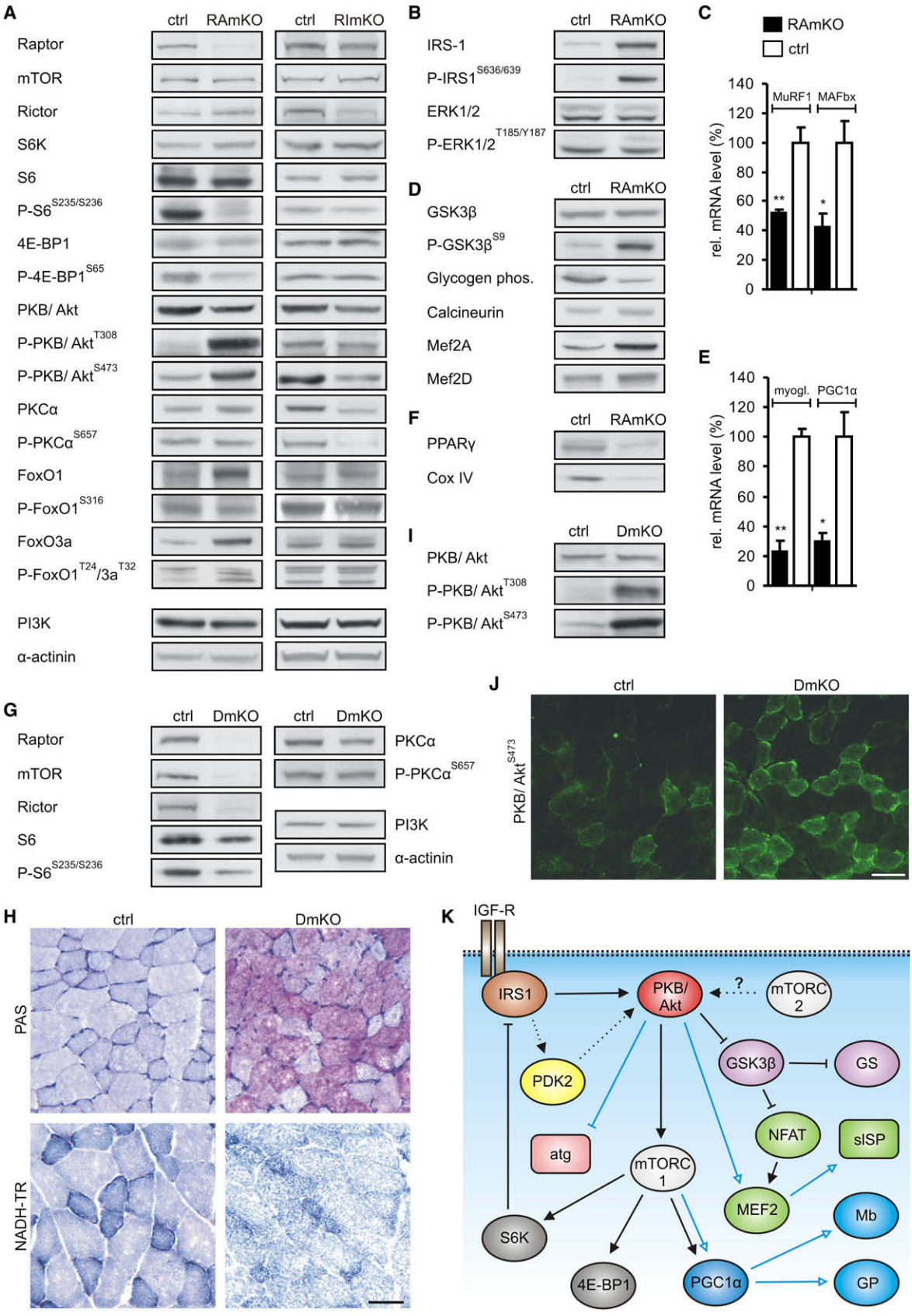
A
ctrl
RAmKO
ctrl
RImKO
Raptor
mTOR
Rictor
S6K
S6
P-S6S235/S236
4E-BP1
P-4E-BP1S65
PKB/ Akt
P-PKB/ AktT308
P-PKB/ AktS473
PKCα
P-PKCαS657
FoxO1
P-FoxO1S316
FoxO3a
P-FoxO1T24/3aT32
PI3K
α-actinin
B
ctrl
RAmKO
IRS-1
P-IRS1S636/639
ERK1/2
P-ERK1/2T185/Y187
C
RAmKO
ctrl
MuRF1
MAFbx
rel. mRNA level (%)
D
ctrl
RAmKO
GSK3β
P-GSK3βS9
Glycogen phos.
Calcineurin
Mef2A
Mef2D
E
myogl.
PGC1α
rel. mRNA level (%)
F
ctrl
RAmKO
PPARγ
Cox IV
I
ctrl
DmKO
PKB/ Akt
P-PKB/ AktT308
P-PKB/ AktS473
G
ctrl
DmKO
ctrl
DmKO
Raptor
mTOR
Rictor
S6
P-S6S235/S236
PKCα
P-PKCαS657
PI3K
α-actinin
J
ctrl
DmKO
PKB/ AktS473
H
ctrl
DmKO
PAS
NADH-TR
K
IGF-R
IRS1
PKB/ Akt
?
mTORC 2
PDK2
GSK3β
GS
NFAT
slSP
atg
mTORC 1
MEF2
Mb
S6K
4E-BP1
PGC1α
GP

by calcium-activated processes acting via calcineurin and CaM kinase IV (Wu et al., 2000). In this context it is interesting to note that the increase of the half-relaxation time in RAmKO muscles may result from a lower removal rate of calcium from the myoplasm by the sarcoplasmic reticulum (Gollnick et al., 1991). This prolonged presence of intracellular calcium during contractile activity might contribute to the activation of calcium-dependent signaling pathways and thus to the upregulation of slSP (Figure 5K). On the other hand, it is possible that Mef2 expression is increased because of hyperactivation of PKB/Akt (Wiedmann et al., 2005). Consistent with this notion, failure to induce a pronounced phosphorylation of PKB/Akt in cultured C2C12 myotubes by treatment with rapamycin coincided with unchanged levels of Mef2A and slMHC (Figure S5C).

Raptor Deficiency Affects Protein Synthesis Directly and PKB/Akt Activation Indirectly

Ablation of mTORC1 in skeletal muscles prevented phosphorylation of S6K/S6 and 4EBP1. This branch of the mTOR signaling pathway is characterized best and has been shown to directly control protein synthesis. Impaired efficacy of protein synthesis in postnatal muscle might also be the reason for the muscles being lighter in RAmKO mice. This effect may also contribute to the shift in fiber size distribution toward smaller values. Our data thus implicate mTORC1 in the maintenance of mass even in fully innervated muscle. Therefore, they extend previous results in which mTOR inhibition by rapamycin was shown to prevent compensatory hypertrophy and recovery from atrophy but not to cause atrophy (Bodine et al., 2001). Our results are also consistent with the findings that skeletal muscles of S6K1-deficient mice are atrophic (Ohanna et al., 2005). The difference in weight of the RAmKO mice became significant only after the age of approximately 2 months, suggesting that the absence of raptor might be compensated for during early periods of muscle growth. One compensatory mechanism could be PKB/Akt-mediated phosphorylation of GSK3β as inhibition of GSK3β has been shown to cause hypertrophy in cultured C2C12 myotubes (Rommel et al., 2001). We also provide evidence that the lack of S6K activation in RAmKO mice is responsible for the hyperphosphorylation of PKB/Akt on Thr308 and Ser473 as levels of IRS-1 were highly increased. Activation of S6K has been shown to decrease the levels of IRS-1 (reviewed in Manning, 2004). Interestingly, the same hyperactivation of PKB/Akt is seen in mice with an adipocyte-specific ablation of *raptor* (Polak et al., 2008).

Raptor-Deficient Skeletal Muscles Are Small, despite High Energy Consumption

Whereas changes in mitochondrial content and function might be based on a direct influence of mTORC1 (Figure 5K), other aspects such as the loss of adipose tissue are probably a consequence of the hyperactivation of PKB/Akt. Muscle-specific overexpression of a constitutively active form of PKB/Akt causes pronounced hypertrophy (Izumiya et al., 2008). Concomitantly with the hypertrophy, mice are lean and do not become obese on a high-fat diet (Izumiya et al., 2008). In the RAmKO mice, PKB/Akt was hyperactive resulting in mice that had much less fat than control mice on a normal chow diet (Table 1) or on a high-fat diet (K.R., C.F.B., and M.A.R., unpublished observation). In contrast to mice that express the constitutively active form of PKB/Akt, lack of mTORC1 prevented the "translation" of PKB/Akt activation into muscle hypertrophy in RAmKO mice. Thus, RAmKO mice behave metabolically like mice that overexpress activated PKB/Akt but lack the hypertrophic effect on muscle. We hypothesize that the metabolic phenotype of being lean is due to the high need of muscles for glucose because of their high glycogen storage capability and their low capacity for oxidative phosphorylation. If the muscle of RAmKO mice acts as such a global glucose sink, non-muscle tissues may have to use alternative energy sources such as fatty acids. This, in turn, could result in an increased release and mobilization of fatty acids from adipose tissue. The high content of glycogen is probably based on the hyperactivation of PKB/Akt, which inhibits GSK3β, which in turn releases inhibition of glycogen synthase (Figure 5H). In addition, inhibition of GSK3β also lowers phosphorylation of NFATc and thus prolongs its activity in the nucleus (Beals et al., 1997). NFATc transcription factors, which are also targets of calcineurin (see above), are known to contribute to fiber type selection (reviewed in Wu et al., 2007). Thus, changes in NFATc activity may add to the expression of structural proteins indicative of slow-twitch muscle.

Hyperactivation of PKB/Akt Does Not Require rictor/mTORC2

Our data strongly indicate that the absence of the S6K-mediated inhibitory feedback caused phosphorylation of PKB/Akt on Thr308 and Ser473 in RAmKO mice. While phosphorylation on Thr308 is mediated by 3-phosphoinositide-dependent kinase (PDK1; Alessi et al., 1997), mTORC2 has been shown to phosphorylate PKB/Akt on Ser473 (Sarbassov et al., 2005). Consistent with such a role for mTORC2, we and others observed a

Figure 5. Biochemical Characterization

(A, B, D, and F) Western blot analysis of soleus muscle from 90-day-old RAmKO, RImKO, and control mice using antibodies directed against the proteins indicated (for details see Experimental Procedures). Equal amount of protein was loaded in each lane. Antibodies to α-actinin and PI3K were in addition used as loading controls.

(C and E) Relative mRNA levels of MuRF1, MAFbx, myoglobin (myogl.), and PGC1α in soleus muscle of 90-day-old RAmKO or control mice. Values obtained in controls were set to 100% (n = 3).

(G and I) Western blot analysis of soleus muscle from 60-day-old DmKO and control mice.

(H) PAS and NADH-TR staining on cross-sections of *triceps* muscles from 50-day-old DmKO and control mice.

(J) Immunostaining with antibodies specific for P-PKB/Akt^{S473} using cross-sections of 60-day-old DmKO and control mice.

(K) Schematic of the interactions contributing to the phenotype of RAmKO mice. Signaling pathway downstream of the insulin/IGF receptor is shown. Blue arrows with open arrowheads represent interactions that affect gene transcription; black symbols represent regulation on the protein level that activates or inhibits the targets. Abbreviations are as follows: atg: atrogenes (MuRF1 and MAFbx); GP: glycogen phosphorylase; GS: glycogen synthase; IGF-R: IGF receptor; Mb: myoglobin; slSP: slow structural proteins.

Data (C and E) represent means ± SEM. Scale bars (H and J): 50 μm. p values are $^{**}p < 0.01$; $^{*}p < 0.05$.

decrease in Ser473 phosphorylation in mice deficient for rictor (Figure 5; Shiota et al., 2006; Guertin et al., 2006; Kumar et al., 2008). We now show that, unexpectedly, muscles from mice lacking both mTORC1 and mTORC2 still showed a marked increase in PKB/Akt phosphorylation on both Thr308 and Ser473. Thus, mTORC2 is not required to phosphorylate PKB/Akt on Ser473 in vivo, indicating that skeletal muscles express a PDK2 distinct from mTORC2. A candidate for this kinase is DNA-dependent protein kinase (DNA-PK), which has been shown to phosphorylate PKBα/Akt1 in cells that are deficient for rictor in response to DNA damage (Bozulic et al., 2008). DNA-PK and PKB/Akt are localized in the nucleus of embryonic fibroblasts upon DNA damage (Bozulic et al., 2008). However, PKB/Akt phosphorylated on Ser473 in DmKO mice was expressed along the sarcolemma and not specifically localized in myonuclei. Several additional proteins have been postulated to act as PDK2, some of which are expressed in skeletal muscle and are localized to the sarcolemma (see Bayascas and Alessi, 2005 for a review).

In summary, our data show that mTORC1 is important for the function and maintenance of skeletal muscle. We provide evidence that the different aspects of the phenotype observed in RAmKO mice are probably based on the direct effect of mTORC1 on its downstream targets S6K and 4EBP1, on the function of mTORC1 to regulate mitochondrial biogenesis and function via PGC1α, or on an indirect effect on its upstream component PKB/Akt. Our data also suggest that long-term treatment with high doses of rapamycin may have detrimental effects on muscle function.

EXPERIMENTAL PROCEDURES

Antibodies

Rabbit polyclonal antibodies are as follows: 4E-BP1 (Phas-I) from Zymed, ERK1&2 pan and ERK1&2 (pTpY185/187) from Biosource, FoxO1a and FoxO1a (phospho S319) from Abcam, P-PKCα (Ser657) and Troponin T-SS (H-55) from Santa Cruz, Phospho-4E-BP1 (Ser65), PAN-actin, Akt, Phospho-Akt (Thr308), Pan-Calcineurin A, Phospho-FoxO1 (Thr24)/FoxO3a (Thr32), Phospho-GSK-3β (Ser9), Phospho-IRS-1 (S636/639), MEF2A, mTOR, PKCα, S6 Ribosomal Protein, Phospho-S6 Ribosomal Protein (Ser235/236), and p70 S6 kinase from Cell Signaling. Rabbit monoclonal antibodies are as follows: β-actin, Phospho-Akt (Ser473), Cox IV, FoxO3a (75D8), GSK-3β, IRS-1, PI3 Kinase p85, Raptor, and Rictor from Cell Signaling and PPARγ from Santa Cruz. Mouse monoclonal antibodies are as follows: α-actinin and myosin (skeletal, slow) from sigma and β-tubulin and Mef2D from BD Biosciences. Goat polyclonal antibody are as follows: GP from Santa Cruz.

Tissue Homogenization, Immunoprecipitation, SDS-PAGE, and Western Blot

Muscles frozen in liquid nitrogen were powdered on dry ice, then transferred to cold RIPA buffer supplemented with 1% Triton-X, 10% glycerol, protease inhibitor cocktail tablets (Roche), and phosphatase inhibitor cocktail I and II (Sigma). Cell lysates were incubated on ice for 2 hr, sonicated two times for 15 s and centrifuged at 13,600 g for 30 min at 4°C. Cleared lysates were then used to determine total protein levels (BCA Protein Assay, Pierce). After dilution with sample buffer, equal protein amounts were loaded onto SDS gels.

Histology and Immunohistochemistry

Muscles frozen in liquid nitrogen-cooled isopentane were fixed with 2% PFA and cut into 12 μm cross-sections. Cross-sections were permeabilized with 1% Triton/PBS for 5 min, washed with 100 mM glycine/PBS for 15 min, blocked with 1% BSA/PBS for 30 min, and incubated with specific primary antibody overnight at 4°C. Samples were subsequently washed with 1% BSA/PBS, three times for 1 hr, stained with appropriate fluorescently labeled secondary antibodies for 1 hr at room temperature. After washing with PBS, samples were mounted with Citifluor (Citifluor Ltd). General histology on cross-sections was performed using hematoxylin and eosin (H&E; Merck, Rayway, NJ, USA). NADH staining was done as described (Dunant et al., 2003). Periodic acid-Schiff staining (PAS staining system, Sigma) was performed according to the manufacturer's instruction. After H&E, NADH, and PAS staining, samples were dehydrated and mounted with DePeX mounting medium (Gurr, BDH).

SUPPLEMENTAL DATA

Supplemental Data include Supplemental Experimental Procedures, five figures, and one table and can be found with this article online at http://www.cellmetabolsim.org/supplemental/S1550-4131(08)00320-3.

ACKNOWLEDGMENTS

We thank people of the Transgenic Mouse Core Facility of the University of Basel, in particular D. Klewe Nebenius, for their help in generating the floxed mice. We are indebted to Drs. A. Felley and T. Pedrazzini at the Rodent Cardiovascular Assessment Facility of the University of Lausanne for echocardiography measurements and U. Sauder from the Microscopy Center of the University of Basel for assistance with electron microscopy. We thank Drs. D. Glass, T. Meier, and M. Sandri for reading the manuscript. This work was supported by the Cantons of Basel-Stadt and Baselland, grants from the Swiss National Science Foundation (M.N.H. and M.A.R.), the Association Francaise contres les Myopathies (F.Z.), and the Swiss Foundation for Research on Muscle Disease (M.A.R.). C.F.B. is a recipient of a fellowship from The Roche Research Foundation.

Received: June 8, 2008
Revised: August 15, 2008
Accepted: October 7, 2008
Published: November 4, 2008

REFERENCES

Alessi, D.R., James, S.R., Downes, C.P., Holmes, A.B., Gaffney, P.R., Reese, C.B., and Cohen, P. (1997). Characterization of a 3-phosphoinositide-dependent protein kinase which phosphorylates and activates protein kinase Balpha. Curr. Biol. *7*, 261–269.

Austyn, J.M., and Gordon, S. (1981). F4/80, a monoclonal antibody directed specifically against the mouse macrophage. Eur. J. Immunol. *11*, 805–815.

Bassel-Duby, R., and Olson, E.N. (2006). Signaling pathways in skeletal muscle remodeling. Annu. Rev. Biochem. *75*, 19–37.

Bayascas, J.R., and Alessi, D.R. (2005). Regulation of Akt/PKB Ser473 phosphorylation. Mol. Cell *18*, 143–145.

Beals, C.R., Sheridan, C.M., Turck, C.W., Gardner, P., and Crabtree, G.R. (1997). Nuclear export of NF-ATc enhanced by glycogen synthase kinase-3. Science *275*, 1930–1934.

Bodine, S.C., Stitt, T.N., Gonzalez, M., Kline, W.O., Stover, G.L., Bauerlein, R., Zlotchenko, E., Scrimgeour, A., Lawrence, J.C., Glass, D.J., and Yancopoulos, G.D. (2001). Akt/mTOR pathway is a crucial regulator of skeletal muscle hypertrophy and can prevent muscle atrophy in vivo. Nat. Cell Biol. *3*, 1014–1019.

Bozulic, L., Surucu, B., Hynx, D., and Hemmings, B.A. (2008). PKBalpha/Akt1 acts downstream of DNA-PK in the DNA double-strand break response and promotes survival. Mol. Cell *30*, 203–213.

Cunningham, J.T., Rodgers, J.T., Arlow, D.H., Vazquez, F., Mootha, V.K., and Puigserver, P. (2007). mTOR controls mitochondrial oxidative function through a YY1-PGC-1alpha transcriptional complex. Nature *450*, 736–740.

Dunant, P., Larochelle, N., Thirion, C., Stucka, R., Ursu, D., Petrof, B.J., Wolf, E., and Lochmuller, H. (2003). Expression of dystrophin driven by the 1.35-kb MCK promoter ameliorates muscular dystrophy in fast, but not in slow muscles of transgenic mdx mice. Mol. Ther. *8*, 80–89.

Glass, D.J. (2005). Skeletal muscle hypertrophy and atrophy signaling pathways. Int. J. Biochem. Cell Biol. *37*, 1974–1984.

Gollnick, P.D., Korge, P., Karpakka, J., and Saltin, B. (1991). Elongation of skeletal muscle relaxation during exercise is linked to reduced calcium uptake by the sarcoplasmic reticulum in man. Acta Physiol. Scand. *142*, 135–136.

Guertin, D.A., Stevens, D.M., Thoreen, C.C., Burds, A.A., Kalaany, N.Y., Moffat, J., Brown, M., Fitzgerald, K.J., and Sabatini, D.M. (2006). Ablation in mice of the mTORC components raptor, rictor, or mLST8 reveals that mTORC2 is required for signaling to Akt-FOXO and PKCalpha, but not S6K1. Dev. Cell *11*, 859–871.

Handschin, C., Chin, S., Li, P., Liu, F., Maratos-Flier, E., Lebrasseur, N.K., Yan, Z., and Spiegelman, B.M. (2007). Skeletal muscle fiber-type switching, exercise intolerance, and myopathy in PGC-1alpha muscle-specific knock-out animals. J. Biol. Chem. *282*, 30014–30021.

Harrington, L.S., Findlay, G.M., Gray, A., Tolkacheva, T., Wigfield, S., Rebholz, H., Barnett, J., Leslie, N.R., Cheng, S., Shepherd, P.R., et al. (2004). The TSC1–2 tumor suppressor controls insulin-PI3K signaling via regulation of IRS proteins. J. Cell Biol. *166*, 213–223.

Heitman, J., Movva, N.R., and Hall, M.N. (1991). Targets for cell cycle arrest by the immunosuppressant rapamycin in yeast. Science *253*, 905–909.

Izumiya, Y., Hopkins, T., Morris, C., Sato, K., Zeng, L., Viereck, J., Hamilton, J.A., Ouchi, N., LeBrasseur, N.K., and Walsh, K. (2008). Fast/Glycolytic muscle fiber growth reduces fat mass and improves metabolic parameters in obese mice. Cell Metab. *7*, 159–172.

Jacinto, E., Loewith, R., Schmidt, A., Lin, S., Ruegg, M.A., Hall, A., and Hall, M.N. (2004). Mammalian TOR complex 2 controls the actin cytoskeleton and is rapamycin insensitive. Nat. Cell Biol. *6*, 1122–1128.

Kumar, A., Harris, T.E., Keller, S.R., Choi, K.M., Magnuson, M.A., and Lawrence, J.C., Jr. (2008). Muscle-specific deletion of rictor impairs insulin-stimulated glucose transport and enhances Basal glycogen synthase activity. Mol. Cell. Biol. *28*, 61–70.

Laws, N., and Hoey, A. (2004). Progression of kyphosis in mdx mice. J. Appl. Physiol. *97*, 1970–1977.

Leone, T.C., Lehman, J.J., Finck, B.N., Schaeffer, P.J., Wende, A.R., Boudina, S., Courtois, M., Wozniak, D.F., Sambandam, N., Bernal-Mizrachi, C., et al. (2005). PGC-1alpha deficiency causes multi-system energy metabolic derangements: muscle dysfunction, abnormal weight control and hepatic steatosis. PLoS Biol. *3*, e101. 10.1371/journal.pbio.0030101.

Lin, J., Wu, H., Tarr, P.T., Zhang, C.Y., Wu, Z., Boss, O., Michael, L.F., Puigserver, P., Isotani, E., Olson, E.N., et al. (2002). Transcriptional co-activator PGC-1 alpha drives the formation of slow-twitch muscle fibres. Nature *418*, 797–801.

Manning, B.D. (2004). Balancing Akt with S6K: implications for both metabolic diseases and tumorigenesis. J. Cell Biol. *167*, 399–403.

Ohanna, M., Sobering, A.K., Lapointe, T., Lorenzo, L., Praud, C., Petroulakis, E., Sonenberg, N., Kelly, P.A., Sotiropoulos, A., and Pende, M. (2005). Atrophy of S6K1(−/−) skeletal muscle cells reveals distinct mTOR effectors for cell cycle and size control. Nat. Cell Biol. *7*, 286–294.

Pallafacchina, G., Calabria, E., Serrano, A.L., Kalhovde, J.M., and Schiaffino, S. (2002). A protein kinase B-dependent and rapamycin-sensitive pathway controls skeletal muscle growth but not fiber type specification. Proc. Natl. Acad. Sci. USA *99*, 9213–9218.

Polak, P., Cybulski, N., Feige, J.N., Auwerx, J., Ruegg, M.A., and Hall, M.N. (2008). Adipose-specific knockout of raptor results in lean mice with enhanced mitochondrial respiration. Cell Metab. *8*, this issue, 399–410.

Popovic, Z.B., Sun, J.P., Yamada, H., Drinko, J., Mauer, K., Greenberg, N.L., Cheng, Y., Moravec, C.S., Penn, M.S., Mazgalev, T.N., and Thomas, J.D. (2005). Differences in left ventricular long-axis function from mice to humans follow allometric scaling to ventricular size. J. Physiol. *568*, 255–265.

Potthoff, M.J., Wu, H., Arnold, M.A., Shelton, J.M., Backs, J., McAnally, J., Richardson, J.A., Bassel-Duby, R., and Olson, E.N. (2007). Histone deacetylase degradation and MEF2 activation promote the formation of slow-twitch myofibers. J. Clin. Invest. *117*, 2459–2467.

Ringelmann, B., Roder, C., Hallmann, R., Maley, M., Davies, M., Grounds, M., and Sorokin, L. (1999). Expression of laminin alpha1, alpha2, alpha4, and alpha5 chains, fibronectin, and tenascin-C in skeletal muscle of dystrophic 129ReJ dy/dy mice. Exp. Cell Res. *246*, 165–182.

Rodriguez, C.I., Buchholz, F., Galloway, J., Sequerra, R., Kasper, J., Ayala, R., Stewart, A.F., and Dymecki, S.M. (2000). High-efficiency deleter mice show that FLPe is an alternative to Cre-loxP. Nat. Genet. *25*, 139–140.

Rommel, C., Bodine, S.C., Clarke, B.A., Rossman, R., Nunez, L., Stitt, T.N., Yancopoulos, G.D., and Glass, D.J. (2001). Mediation of IGF-1-induced skeletal myotube hypertrophy by PI(3)K/Akt/mTOR and PI(3)K/Akt/GSK3 pathways. Nat. Cell Biol. *3*, 1009–1013.

Sakamoto, K., and Goodyear, L.J. (2002). Invited review: intracellular signaling in contracting skeletal muscle. J. Appl. Physiol. *93*, 369–383.

Sandri, M., Sandri, C., Gilbert, A., Skurk, C., Calabria, E., Picard, A., Walsh, K., Schiaffino, S., Lecker, S.H., and Goldberg, A.L. (2004). Foxo transcription factors induce the atrophy-related ubiquitin ligase atrogin-1 and cause skeletal muscle atrophy. Cell *117*, 399–412.

Sarbassov, D.D., Ali, S.M., Kim, D.H., Guertin, D.A., Latek, R.R., Erdjument-Bromage, H., Tempst, P., and Sabatini, D.M. (2004). Rictor, a novel binding partner of mTOR, defines a rapamycin-insensitive and raptor-independent pathway that regulates the cytoskeleton. Curr. Biol. *14*, 1296–1302.

Sarbassov, D.D., Guertin, D.A., Ali, S.M., and Sabatini, D.M. (2005). Phosphorylation and regulation of Akt/PKB by the rictor-mTOR complex. Science *307*, 1098–1101.

Schieke, S.M., Phillips, D., McCoy, J.P., Jr., Aponte, A.M., Shen, R.F., Balaban, R.S., and Finkel, T. (2006). The mammalian target of rapamycin (mTOR) pathway regulates mitochondrial oxygen consumption and oxidative capacity. J. Biol. Chem. *281*, 27643–27652.

Schwander, M., Leu, M., Stumm, M., Dorchies, O.M., Ruegg, U.T., Schittny, J., and Muller, U. (2003). Beta1 integrins regulate myoblast fusion and sarcomere assembly. Dev. Cell *4*, 673–685.

Sewry, C.A., Muller, C., Davis, M., Dwyer, J.S., Dove, J., Evans, G., Schroder, R., Furst, D., Helliwell, T., Laing, N., and Quinlivan, R.C. (2002). The spectrum of pathology in central core disease. Neuromuscul. Disord. *12*, 930–938.

Shiota, C., Woo, J.T., Lindner, J., Shelton, K.D., and Magnuson, M.A. (2006). Multiallelic disruption of the rictor gene in mice reveals that mTOR complex 2 is essential for fetal growth and viability. Dev. Cell *11*, 583–589.

Song, X.M., Ryder, J.W., Kawano, Y., Chibalin, A.V., Krook, A., and Zierath, J.R. (1999). Muscle fiber type specificity in insulin signal transduction. Am. J. Physiol. *277*, R1690–R1696.

Sorokin, L.M., Pausch, F., Frieser, M., Kroger, S., Ohage, E., and Deutzmann, R. (1997). Developmental regulation of the laminin alpha5 chain suggests a role in epithelial and endothelial cell maturation. Dev. Biol. *189*, 285–300.

Stitt, T.N., Drujan, D., Clarke, B.A., Panaro, F., Timofeyva, Y., Kline, W.O., Gonzalez, M., Yancopoulos, G.D., and Glass, D.J. (2004). The IGF-1/PI3K/Akt pathway prevents expression of muscle atrophy-induced ubiquitin ligases by inhibiting FOXO transcription factors. Mol. Cell *14*, 395–403.

Treves, S., Jungbluth, H., Muntoni, F., and Zorzato, F. (2008). Congenital muscle disorders with cores: the ryanodine receptor calcium channel paradigm. Curr. Opin. Pharmacol. *8*, 319–326.

Tsang, C.K., Qi, H., Liu, L.F., and Zheng, X.F. (2007). Targeting mammalian target of rapamycin (mTOR) for health and diseases. Drug Discov. Today *12*, 112–124.

Um, S.H., Frigerio, F., Watanabe, M., Picard, F., Joaquin, M., Sticker, M., Fumagalli, S., Allegrini, P.R., Kozma, S.C., Auwerx, J., and Thomas, G. (2004). Absence of S6K1 protects against age- and diet-induced obesity while enhancing insulin sensitivity. Nature *431*, 200–205.

Wende, A.R., Schaeffer, P.J., Parker, G.J., Zechner, C., Han, D.H., Chen, M.M., Hancock, C.R., Lehman, J.J., Huss, J.M., McClain, D.A., et al. (2007). A Role for the transcriptional coactivator PGC-1{alpha} in muscle refueling. J. Biol. Chem. *282*, 36642–36651.

Wiedmann, M., Wang, X., Tang, X., Han, M., Li, M., and Mao, Z. (2005). PI3K/Akt-dependent regulation of the transcription factor myocyte enhancer

factor-2 in insulin-like growth factor-1- and membrane depolarization-mediated survival of cerebellar granule neurons. J. Neurosci. Res. *81*, 226–234.

Winkel, L.P., Hagemans, M.L., van Doorn, P.A., Loonen, M.C., Hop, W.J., Reuser, A.J., and van der Ploeg, A.T. (2005). The natural course of non-classic Pompe's disease; a review of 225 published cases. J. Neurol. *252*, 875–884.

Wu, H., Naya, F.J., McKinsey, T.A., Mercer, B., Shelton, J.M., Chin, E.R., Simard, A.R., Michel, R.N., Bassel-Duby, R., Olson, E.N., and Williams, R.S. (2000). MEF2 responds to multiple calcium-regulated signals in the control of skeletal muscle fiber type. EMBO J. *19*, 1963–1973.

Wu, H., Peisley, A., Graef, I.A., and Crabtree, G.R. (2007). NFAT signaling and the invention of vertebrates. Trends Cell Biol. *17*, 251–260.

Wullschleger, S., Loewith, R., and Hall, M.N. (2006). TOR signaling in growth and metabolism. Cell *124*, 471–484.